Residual Stress in the Duplex Stainless Steel Sandvik SAF 2205 after Annealing and Tumbling

C.-O. A. Olsson

The effect of tumbling on the individual phases in the duplex stainless steel Sandvik SAF 2205 (EN 1.4462) was examined by X-ray Diffraction. In addition, tie line alloys with compositions close to those of the respective phases were used. The use of tie line alloys makes it possible to compare the tumbling response as a function of microstructure, including the interaction between austenite and ferrite. It was established that annealing and tumbling both induced stress in duplex stainless steels. A standard annealing procedure created a surface with a neutral average stress state, but with compensating tensile (austenite) and compressive (ferrite) contributions from the respective phases. Tumbling of the steel surfaces led to an evening out of the residual stress between the phases. Tumbling of the ferritic sample created higher stress levels, possibly explained by fewer available slip systems. For the duplex metal, microstrain values estimated from line broadening were consistently higher than for the respective single phase samples.

KEYWORDS: DUPLEX STAINLESS STEEL, AUSTENITE, FERRITE, TUMBLING, X-RAY DIFFRACTION, RESIDUAL STRESS, SURFACE TREATMENT

INTRODUCTION

Many properties of duplex stainless steels can be understood from their dual phase structure: they have a mechanical strength almost twice that of austenitic materials, they have a corrosion resistance that in many cases surpasses what would be expected from a single phase alloy with similar composition; the dual phase arrangement also provides an excellent resistance against stress corrosion cracking. In this paper, it was chosen to study the residual stresses created when the surface of a duplex stainless steel is subjected to a comparatively mild surface treatment - tumbling.

Tumbling, sometimes also barreling, is a method for surface treatment that consists of placing the piece to be treated in a drum together with a tumbling medium which could be wet or dry, and consist of a mix of liquid and solid pieces, typically sand, granite, ceramics or synthetics. As the drum turns, the content is moved around and the surface is eroded. Compared to alternate processes such as shot-peening, tumbling is a milder method. For a stainless steel, a tumbled surface would normally have compressive residual stress, which typically is somewhat lower than when using shot-peening or sand blasting. The residual stress condition in a martensitic steel after tumbling was studied by Olsson et al., comparing laboratory X-ray with a synchrotron method [1]. X-Ray Diffraction is a well established tool for investigating residual stress. As the diffraction peaks for ferrite and austenite are separated, it is possible to measure strain in each individual phase without resolving them laterally. Recent overviews of residual stress measurements have been written by Genzel [2] and Benediktovitch et al. [3]. Residual stress is normally divided into three types: macro stress (σ^{I}), meso stress (σ^{II}), sometimes micro-stress, is the average stress in a crystallite, and nano stress (σ^{III}), which is the deviation from the average stress within a crystallite. In this paper, σ^{I} and σ^{II} were estimated from peak positions in the different phases, using a parallel beam configuration. In addition, line profile broadening was used to estimate a microstrain contribution. For this type of analysis, a high-resolution Bragg Brentano setup was used.

For duplex stainless steels, the stress partitioning between the different phases in the bulk material has been studied previously with experimental as well as modeling methods. Johansson et al. studied the evolution of the residual stress state during loading, combining experiments with a finite element analysis of the different phases [4]. Lillbacka et al. used a similar approach to investigate cyclic stress-strain behavior and load sharing

Claes-Olof A. Olsson

Sandvik Materials Technology,
SE-811 81 Sandviken, Sweden

[5]. The interaction between phase stress and grain orientation dependent stress was investigate in detail by Jia et al, using neutron diffraction [6]. The surface integrity of duplex stainless steels after different types of machining operations was investigated by Zhou et al, with the objective to better understand the influence of surface condition on stress corrosion cracking [7, 8]. Compressive residual stress is frequently induced deliberately in steel surfaces to improve fatigue life. Tensile strain in the surface is normally less desirable, since it may facilitate crack initiation. The surface region with compressive strain induced by tumbling normally extends some 5 - 20 µm into the material [1]; the depth depends on tumbling as well as material parameters. In this paper, we study the interaction between the ferritic and austenitic phase in a duplex material, by imposing a mild mechanical deformation on the surface. Three sample types were used for this purpose: a single phase austenite, a single phase ferrite, as well as a duplex stainless steel. The single phase samples were designed to make their respective compositions close to those of the duplex material. With this experiment design, it is possible to assess the different contributions from the austenite and ferrite and gain a better understanding of tumbling response, not only for classic duplex materials, but also for ferritic materials with residual austenite, and vice versa.

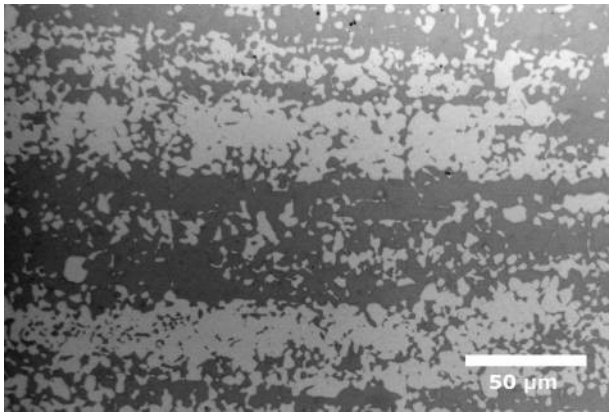

Annealed

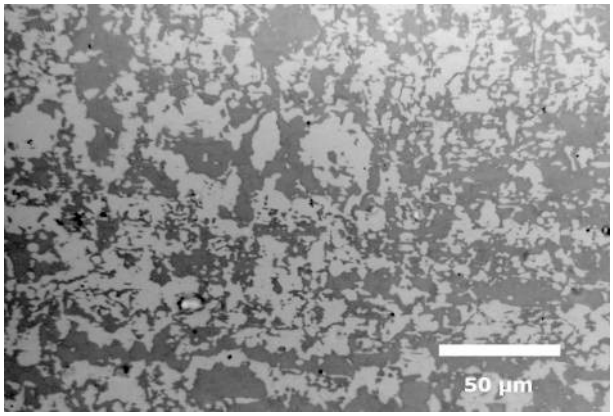

Cold Rolled

Fig. 1 - Longitudinal cross sections after electropolishing and subsequent etching in Murakami's etchant, recorded at 500X. The ferritic regions appear as dark contrast in the images.

Tab.1 - Compositions (wt%) of the samples and, determined with SEM-EDS for the major alloying elements, and with EPMA for nitrogen.

Sample	Phase	Cr	Fe	Ni	Mo	N
100% Austenite	γ	20.5	67.0	9.1	2.1	0.11
100% Ferrite	α	24.5	66.8	4.2	3.5	0.00
2205 Annealed	γ	21.4	69.2	6.1	2.5	0.38
	α	23.4	68.2	4.4	3.4	0.09
2205 Cold Rolled	γ	21.6	69.2	6.1	2.6	0.22
	α	23.3	68.3	4.5	3.5	0.03

Tab.2 - Phase fractions for the different duplex samples used. The values are averages from five images. Uncertainties are given as one standard deviation.

Sample	Condition	Ferrite Fraction, %
	Annealed	52 ± 5
	Cold Rolled	47 ± 6

EXPERIMENTAL

Material and sample preparation

The duplex samples of grade Sandvik SAF 2205 (EN 1.4462) were taken from the production conditions: as annealed and as cold rolled. For brevity, the commercial material is referred to as 2205 below. The single phase samples were heat treated at 1050°C, water quenched and cut to size. The compositions of the samples and phases are given in table 1. For the major elements, SEM-EDS was used. The quantification was based on a powder metallurgical compound standard. For nitrogen, the compositions were determined with a dedicated Electron Probe Microanalyzer (EPMA), using a calibration line consisting of four samples with different nitrogen concentrations. The annealed and cold-rolled commercial materials originated from two different heats, but the phase compositions were close. Especially for the cold rolled material, the structure was very fine, with grain sizes close to the analytical resolution of the SEM/EDS technique at 20 kV. To remove points with lateral phase overlap, some 200 datapoints were analyzed, and the chromium signal was used to sort datapoints into ferritic and austenic by a histogram. Overlapping points were not part of the evaluation.

Tumbling was performed by Trumlingsaktiebolaget in Solna, Sweden. The steel samples were tumbled together with chips and water for a total of 7.5 hours. This resulted in a clean and matte surface.

Electropolishing was performed prior to X-ray Diffraction to remove any residual stress introduced by the grinding and polishing procedure. This was done with a Struers Lectropol 5, applying a 35V tension and a pump speed of 15 - 20 for 30 s. The electrolyte used was a 3 M H_2SO_4 in ethanol, cooled to -20°C. The polished surface was 1 cm^2, and the resulting current varied between 1.2 and 1.6 A. The electropolishing resulted in a mirror finish surface.

X-Ray Diffraction

Two diffractometers were used to record macro and micro stresses. The macro stresses were determined by applying the $\sin^2\psi$ method to the austenite (2 2 0) and ferrite (2 1 1) peaks. The stress levels within the grains were calculated from the respective phases using peak widths determined by a le Bail refinement.

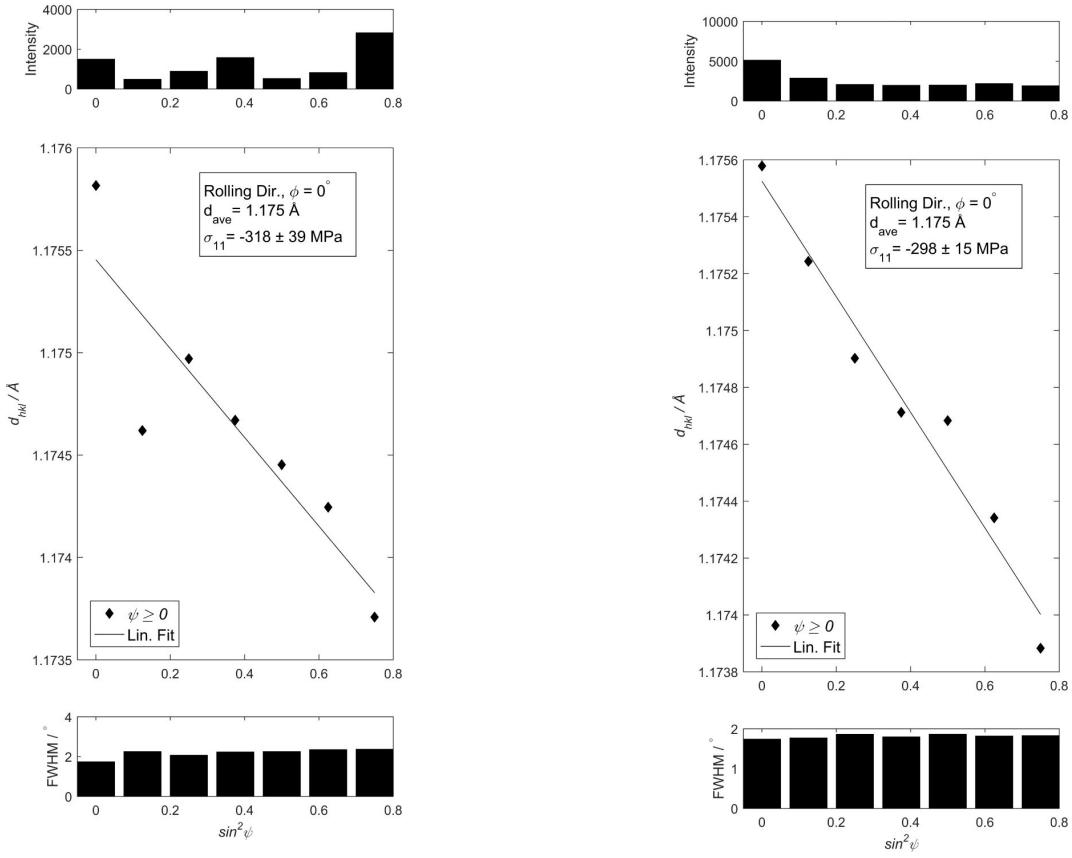

Fig.2 - Example d vs. $\sin^2\psi$ plots for ferritic peaks on the (2 1 1) reflection; cold rolled (left) and annealed (right) after electropolishing, both measured in the rolling direction.

Macro Stress Measurements
The diffractometer used was a Bruker D8 Discover, installed in 2001, equipped with a Cr K_α source, a polycapillary attachment and a LynxEye silicon strip detector. The samples were fixed on a 5 axis Eulerian cradle and the diameter of the incoming X-ray beam was 2 mm. Two perpendicular directions were measured, and a total of 7 χ angles ranging from 0 to 60° were used, with a linear distribution in $\sin^2\psi$ i.e. [0 - 0.125 - 0.25 - 0.375 - 0.5 - 0.625 - 0.75]. The elastic constants as supplied by the diffractometer manufacturer are given in table 3. The stress evaluation was performed using in-house software.

Tab.3 - Elastic constants used for this paper. The 2θ positions are given for a Cr K_α source

Phase	h k l	2θ	Poisson	Young's Modulus / MPa
Austenite	2 2 0	129°	0.28	207 039
Ferrite	2 1 1	156°	0.28	220 264

Mesoscopic Stress - σ^{II}
The mesoscopic stress σ^{II}, frequently also denoted type II micro stress, for the respective phases was estimated from the equations:

$$\sigma^{Ave} = \sigma^{\gamma} V^{\gamma} + \sigma^{\alpha}(1 - V^{\gamma}) \quad (1)$$

$$\sigma^{II\gamma} = \sigma^{\gamma} - \sigma^{Ave} \quad (2)$$

$$\sigma^{II\alpha} = \sigma^{\alpha} - \sigma^{Ave} \quad (3)$$

More detail on this partitioning can be found in textbooks, for example by Genzel [2] or Hauk [9]. V^{γ} is the volume fraction of austenite phase as measured with image analysis on light optical micrographs, see table 2, and σ^{γ} is the residual stress as measured for the austenitic phase using the d vs. $\sin^2\psi$ method.

Stress Calculated from Line Profile Broadening
Line broadening effects were investigated using a Bruker D8 Discover, installed in 2014, equipped with a Co K_α source. It was operated in a Bragg-Brentano configuration with line focus, giving a 12 mm wide footprint on the sample surface. The incoming beam was parallelized using 2.5° Soller slits on the primary as well as the secondary side. The primary slit opening was set to 0.2°, to make the peaks as narrow whilst maintaining sufficient intensity. As detector, a LynxEye XE silicon strip detector was used. The sample was fixed on a five axis Eulerian cradle with a spinner attachment.

The diffractometer broadening was determined by running a NIST Corund (α-Al_2O_3) SRM 660b, and applying a convolution function to compensate for peak broadening. All evaluation of microstrain was performed in the Bruker Topas 5.0 software. Fundamental parameters were used to approximate the peak shape. The pattern was fitted with an hkl-type phase using the le Bail method, applying a Gaussian-Lorentzian mix to estimate peak shape. As discussed by Genzel in Hauk et al. [9], line profile broadening contains contributions not only from strain, but also from deformation and twinning, as well as the diffracting domain size.

RESULTS

Microstructure
Residual stress measurements were performed on plane sections for all samples, except for the purely ferritic one which was available in bar shape and cut to discs, making both analyzed directions perpendicular to the cast direction. For the commercial grades, micrographs taken on longitudinal cross sections are found in Figure 1. A total of five images were recorded at a magnification of 500X. The preparation started with electropolishing for 30 - 60 s, and then etching in Murakami's etchant. Ferrite fractions, listed in table 2, were calculated from the micrographs using image analysis automated with an Otsu thresholding method; a 50/50 mix of austenite and ferrite was established for all duplex samples.
Residual stress measurements were performed as double samples for all types of surfaces with the d vs $\sin^2\psi$ method. Sample plots can be seen in figure 2, which depict data from the ferritic (2 1 1) reflection for a cold rolled and an annealed

sample, both measurements were taken in the rolling direction. The plots show the intensity distribution (top), lattice parameter (mid), as well as peak width (below) dependence on the angle versus sample surface normal (ψ). If the sample has a strong preferential orientation, it can be seen as intensity variations in the top graph. Both samples in figure 2 show preferential orientations, with a higher amplitude for the annealed sample. The amount of cold deformation in the sample is reflected in the peak width. The cold rolled sample in figure 2a shows significantly broader peaks than those of the annealed variant (2b). The residual strain is calculated from the slope in the d vs $\sin^2\psi$ plot. Both samples showed similar residual stress levels, about -300 MPa of compression. The strain is then converted into stress using the elastic constants given in table 1. Residual stress levels obtained with the d vs $\sin^2\psi$ method for all samples and surface treatments are given in tables 4a (transverse direction) and 4b (rolling direction). Phase separation is obtained by selecting two different diffraction peaks: (2 1 1) for the ferrite and (2 2 0) for the austenite. Tumbling generated a compressive surface stress for all samples. To get an impression of the stress condition at about 100 µm depth, electroplished samples were also analyzed. This procedure necessitates a plane stress condition. For the annealed condition, the austenite and ferrite phases gave rise to a mix of compressive / tensile stresses, resulting in a neutral overall residual stress state.

Tab.4a - Residual stress in the transverse and rolling directions. *Samples A and F are fully austenitic and ferritic samples in annealed condition, with compositions corresponding to the respective phases in the commercial material. †The single phase ferritic sample was cut perpendicular to the rolling direction, hence both analyzed directions are transverse.

Sample	Austenite		Ferrite	
[MPa]	El-Pol	Tumbled	El-Pol	Tumbled
A*	-143±147	-415±28		
	60±290	-485±65		
F*			225±242	-806±63
			129±81	-671±100
F*†			54±2	-784±106
			186±39	-880±45
Cold Rolled	-170±138	-518±73	-184±23	-450±46
	-10±160	-403±40	-192±27	-466±47
Annealed	360±46	-343±34	-428±45	-427±37
	384±12	-368±43	-331±12	-526±60

Tab.4b - Rolling direction

Sample	Austenite		Ferrite	
[MPa]	El-Pol	Tumbled	El-Pol	Tumbled
A*	-224±92	-472±52		
	-110±132	-472±55		
Cold Rolled	81±154	-331±53	-378±30	-548±92
	26±115	-219±63	-341±44	-562±79
Annealed	371±20	-336±53	-327±29	-503±69
	462±64	-355±56	-405±55	-430±33

Strain caused by defects within a grain can be estimated by analyzing peak broadening. After compensating for diffractometer line width, mechanisms that contribute to line broadening include: diffracting domain size, deformation faults and, in fcc material, twinning. If these factors can be kept under control, for example by comparing a duplex material with the corresponding single phase alloys, this type of microstress can be estimated by recording a θ-θ diffractogram in high resolution Bragg-Brentano mode, as depicted in figure. 3. The austenite and ferrite peaks are clearly resolved. Peaks were fitted using fundamental parameters with the le Bail method. The diffractometer peak broadening was recorded on a reference sample of corundum (α-Al_2O_3), NIST 660b, and the reported residual stress was calculated from the additional broadening. The results are found in table 5. For the polished ferritic sample, the preferential orientation resulted in fewer visible peaks, adding uncertainty to the determination of the microstress based on a multi-peak approach. The sample where this effect was dominating is marked "textured".
For both duplex samples, there were no significant differences between the as-tumbled and as-annealed conditions. As expected, the values for cold rolled material were consistently higher than after annealing. In addition, cold rolling produced a higher level of micro stress in the austenite, compared to the ferrite.

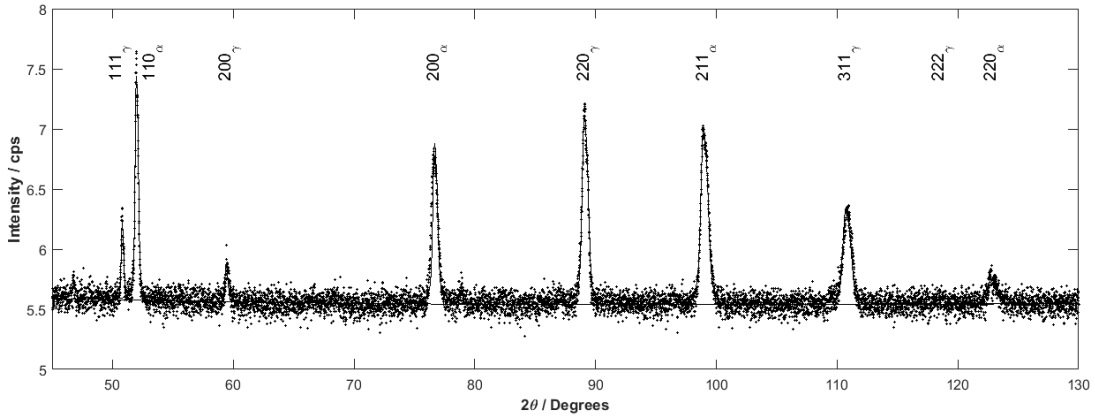

Fig. 3 - Diffractogram from the as annealed duplex sample, showing the acquired diffractogram (dots) together with the background, le Bail fits of the austenite and ferrite phases, as well as the envelope.

Tab. 5 - Microstress estimated from line broadening in austenite and ferrite, before and after tumbling. The stress was obtained using the Young's moduli for austenite and ferrite given in table 1.

Sample	Austenite		Ferrite	
[MPa]	Polished	Tumbled	Polished	Tumbled
A	11	22		
	20	75		
F			104	313
			Textured	369
Cold Rolled	425	412	296	298
	432	434	292	296
Annealed	152	141	155	151
	156	139	151	141

DISCUSSION

To facilitate the interpretation, σ^{II} residual stress distributions were calculated using equations (1-3); the results are shown in figure 4. σ^{II} is the local strain within a grain, so it is logical to separate the figures into the austenitic (a) and ferritic (b) contributions. As the matrix is close to a 50/50 mixture of austenite and ferrite, the residual stress in one phase will mirror that of the other. The austenitic phase was found to be consistently in tension, and the ferritic phase in compression. For both the tumbled and electropolished states, there was a directional dependence with higher stress in the rolling direction.

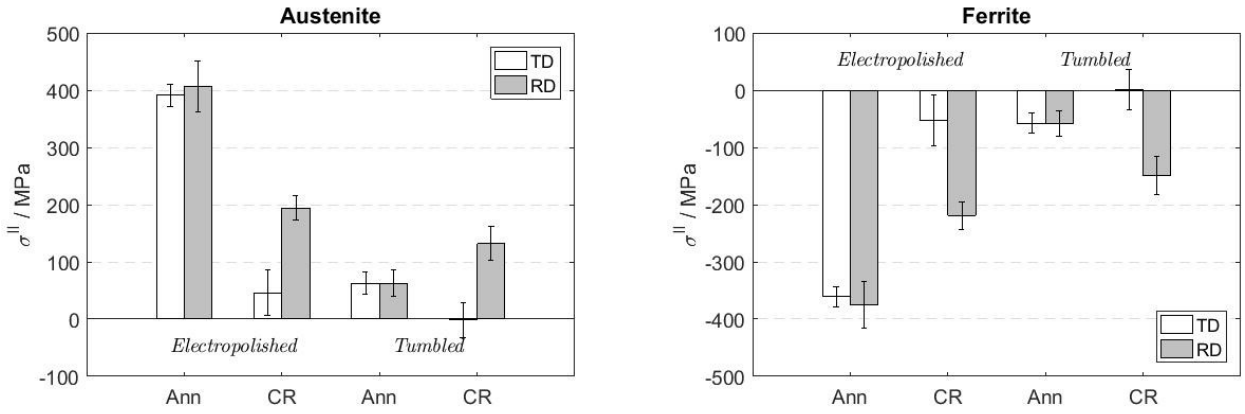

Fig.4 - Calculated (σ^{II}) levels, representing the stress within austenitic (a) and ferritic (b) grains. The error bars represent max and min values.

For the annealed samples, the residual strain levels were higher. As has been pointed out earlier by Johansson et al. [4], this is possible to understand qualitatively by regarding the differences in thermal expansion of the two phases: assume that cooling starts with a neutral stress state at 1070°C, together with a 50/50 phase balance. The same thermal expansion coefficients as used by Jia et al., i.e. $18 \cdot 10^{-6}$ K^{-1} for fcc and $12 \cdot 10^{-6}$ K^{-1} for bcc were used [10]. This gives a stress difference between the phases of 1 GPa, i.e. +500 MPa for the austenite and -500 MPa for the ferrite. This is also in quantitative agreement with the results figure 4. The fact that residual stress arises from differences in thermal expansion between the different phases is further supported by the observation that the residual stress levels are considerably lower in the tie line alloys, see table 4.

The line width analysis showed significantly narrower peaks for the single phase alloys, compared to the corresponding phases in the duplex materials. The state of the art of line width analysis with XRD was reviewed in 2008 by Mittemeijer and Wenzel [11], who discussed the main effects, i.e. size-strain and microstrain broadening. Separating the different contributions to line broadening is not a straight-forward manner, but the use of a duplex material and the corresponding single phase alloys make some of these effects cancel. Typical grain sizes in a duplex stainless steel are normally larger than one µm, which means that their size contribution to peak broadening should be small. Other contributing factors, such as twins in the austenite, and deformation faults in the austenite and ferrite, could be assumed to have the same contribution in a single phase and a duplex material. Hence, microstress values were calculated and are listed in table 5. It was found that the duplex materials showed consistently higher values. One important difference between single phase and duplex materials are the interphase boundaries. It thus seems reasonable to assume that at least a part of this difference could be attributed to lattice strain at these boundaries. Another interesting observation is that the line broadening in the duplex material due to tumbling was close to negligible, whereas there was a marked effect for the purely ferritic samples. This could be related to fewer available slip planes in the bcc structure. Another contributing factor could be that the major part of the deformation in the duplex material is located to the austenite.

It is interesting to compare the values of tie line alloys in table 3, with the σ^{II} levels in figure 4. Whereas the stress levels for ferrite in the duplex sample are consistently compressive,

the single phase ferrite showed tensile stress in absence of mechanical work. As expected, it also showed strong compressive residual stress after tumbling, about -800 MPa. Thus, it is clear that the heating and cooling cycles have a marked influence on the resulting residual stress state, and that the interaction between different phases in a bi-phase material creates a residual stress state that differs from what is obtained for single phase alloys.

CONCLUSIONS

Different types of processing can lead to the creation of internal stress in duplex stainless steels. It was shown that annealing creates a surface with a neutral average stress state, but with compensating tensile (austenite) and compressive (ferrite) stress. Tumbling of the steel surfaces led to an averaging of the residual stress levels in the respective phases. Ferritic phase tumbling created higher stress levels, which could be explained by fewer available slip systems. Strain values estimated from line profile broadening were consistently higher in the duplex materials, compared to single phase alloys with the same composition. One likely contribution to this phenomenon is the lattice strain component in the interphase boundaries.

ACKNOWLEDGEMENTS

The EPXMA analysis was performed by Dr. A. Golpayegani. Dr. A. Hoel contributed with samples and tumbling advice, and Dr. T. Forsman with valuable comments on the script.

REFERENCES

[1] C.-O. A. OLSSON, M. BOSTRÖM, T. BUSLAPS and A. STEUWER, Strain, 51, (2015), p. 71.

[2] C. GENZEL, in Moderne Röntgenbeugung, 2 ed., L. Spiess Editor, Vieweg + Teubner, Wiesbaden (2009). p. 305.

[3] A. BENEDIKTOVITCH, I. FERANCHUK and A. ULYANENKOV, Theoretical Concepts of X-Ray Nanoscale Analysis, p. 318, Springer Verlag, Berlin Heidelberg (2014).

[4] J. JOHANSSON, M. ODÉN and X. H. ZENG, Acta Materialia, 47, (1999), p. 2669.

[5] R. LILLBACKA, G. CHAI, M. EKH, P. LIU, E. JOHNSON and K. RUNESSON, Acta Materialia, 55, (2007), p. 5359.

[6] N. JIA, R. LIN PENG, G. C. CHAI, S. JOHANSSON and Y. D. WANG, Materials Science and Engineering: A, 491, (2008), p. 425.

[7] N. ZHOU, R. PETTERSSON, R. LIN PENG and M. SCHÖNNING, Materials Science and Engineering A, 658, (2016), p. 50.

[8] N. ZHOU, R. L. PENG and R. PETTERSSON, Journal of Materials Processing Technology, 229, (2016), p. 294.

[9] V. HAUK, H. BEHNKEN, C. GENZEL, W. PFEIFER, L. PINTSCHOVIUS, W. REIMERS, E. SCHNEIDER, B. SCHOLTES and W. A. THEINER, Structural and Residual Stress Analysis by Nondestructive Methods, p. 640, Elsevier Science B. V., Amsterdam (1997).

[10] N. JIA, R. L. PENG, Y. D. WANG, G. C. CHAI, S. JOHANSSON, G. WANG and P. K. LIAW, Acta Materialia, 54, (2006), p. 3907.

[11] E. J. MITTEMEIJER and U. WELZEL, Z. Kristallogr., 223, (2008), p. 552.I. GUTIERREZ-URRUTIA and D. RAABE, Acta Mater. 60 (2012), p.5791.